Published in final edited form as:
Neurogastroenterol Motil. 2013 January ; 25(1): 53–e6. doi:10.1111/nmo.12010.

Characterization of the Distal Esophagus High-Pressure Zone with Manometry, Ultrasound and Micro-Computed Tomography

Anil K. Vegesna[1], **Joshua A. Sloan**[5], **Baltej Singh**[1], **Steven J Phillips**[2], **Alan S. Braverman**[2,3], **Mary F. Barbe**[2], **Michael R. Ruggieri Sr.**[2,3,4], and **Larry S. Miller**[1]

[1]Departments of Medicine, Section of Gastroenterology, Philadelphia College of Osteopathic Medicine

[2]Department of Anatomy and Cell Biology, Philadelphia College of Osteopathic Medicine

[3]Department of Urology, Philadelphia College of Osteopathic Medicine

[4]Department of Pharmacology, Philadelphia College of Osteopathic Medicine

[5]Temple University School of Medicine, and the Philadelphia College of Osteopathic Medicine

Abstract

Background—We sought to determine how the individual components of the distal esophagus and proximal stomach form the gastroesophageal junction high-pressure zone (GEJHPZ) anti-reflux barrier.

Methods—An endoscopic ultrasound/manometry catheter was pulled through the proximal stomach and distal esophagus in 20 normal subjects. The axial length and width of individual structures on endoscopic ultrasound were measured. The anatomic orientation of gastroesophageal junction (GEJ) components was examined in two organ donor specimens using micro-computed tomography (micro-CT).

Key Results—The three distinct structures identified within the GEJHPZ, from distal to proximal, were: the gastric clasp and sling muscle fiber complex, crural diaphragm, and lower esophageal circular smooth muscle fibers (LEC). The LEC was statistically significantly thicker than adjacent esophageal muscles. These structures were associated with 3 pressure peaks. The pressure peak produced by the clasp/sling fiber complex often overlapped with the pressure peak from the crural diaphragm. The most proximal peak, associated with the LEC, was significantly greater and bimodal in 9 of 20 subjects. This bimodal LEC pressure peak correlated with two areas of thickened muscle observed with ultrasound. Micro-CT of GEJ from organ donors confirmed the two areas of thickened muscle.

Conclusions and inferences—Three distinct anatomic structures, the clasp and sling muscle fibers, crural diaphragm, and LEC combine to form the anti-reflux barrier of the proximal stomach and distal esophagus. The clasp and sling muscle fibers combine with the crural diaphragm to form a distal pressure profile. The more proximal LEC has a bimodal pressure profile in some patients.

Corresponding author: Dr. Michael R. Ruggieri, Sr., Temple University School of Medicine, 3400 North Broad Street, Philadelphia, PA 19140. rugg@temple.edu telephone: (215) 707-4567 Fax: (215) 707-4565.

Financial Disclosures: None
Conflict of Interest: None

Author Contributions: Study concept and design - AV, LM, MFB, MRR. Acquisition of data, analysis and interpretation of data - AV, AB, LM, MFB, MRR. Drafting of the manuscript - AV, BS, JS, LM, MRR. Critical revision of the manuscript for important intellectual content – AV, LM, MRR. Statistical analysis - AV, JS, LM, MRR. Obtained funding - LM, MRR. Administrative – AV, BS, JS, SJP. Technical or material support - AV, LM, MFB, SJP. Study supervision - LM, MRR.

Keywords

Barrett's Esophagus; Clasp fibers; Endoscopic Ultrasound; Gastroesophageal Reflux Disease; High-Pressure Zone; Lower Esophageal Circular Sphincter; Lower Esophageal Sphincter; Manometry; Micro-CT; Sling fibers; Upper Gastric Sphincter

Introduction

Dysfunction of the gastroesophageal junction high-pressure zone (GEJHPZ) leads to gastroesophageal reflux disease (GERD). Approximately 10–20% of the population in North America and Europe experience weekly symptoms of GERD and this has been increasing over time (1). GERD's sequelae include Barrett's esophagus with an increased risk for esophageal adenocarcinoma. Previous studies described a high-pressure zone (HPZ) that helps prevent reflux of gastric contents into the esophagus. This includes a skeletal muscle component consisting of the crural diaphragm and overlapping, atropine sensitive smooth muscle components (2–10). The wall of the distal esophagus has been documented with endoscopic ultrasound (EUS) to be thicker than wall of the body of the esophagus, indicative of an intrinsic sphincter (11).

In 1979, Liebermann-Meffert *et al.* characterized the clasp and sling muscle fibers in cadavers. They described the sling muscle fibers on the greater curvature of the stomach and the clasp muscle fibers on the lesser curvature, both found within the gastric cardia (13). The clasp and sling muscle fibers have been characterized as having an asymmetric distribution as well as being the major anatomic component within the HPZ (14–16). However, this observation is contrary to other findings, suggesting that multiple anatomic regions generating pressures contribute to the HPZ. As such, it is presumed that the clasp and sling muscle fibers contribute to the overall pressure within the HPZ, but are not the sole influence (12, 15).

By measuring endoluminal pressures before and after either atropine or cis-atracurium administration to differentiate between smooth muscle and skeletal muscle components of the HPZ, we previously identified two pressure peaks associated with the smooth muscle, one distal to the crural diaphragm and one proximal to the crural diaphragm (12). We hypothesized that the distal smooth muscle pressure peak is generated by the clasp and sling fiber complex of the proximal stomach, the skeletal muscle pressure peak is generated by the crural diaphragm, and the more proximal smooth muscle pressure peak is generated by the thickened lower esophageal circular (LEC) smooth muscle fibers (12). We found a decrease in the distal smooth muscle pressure component in subjects with GERD as compared with normal subjects and concluded that a defect in this clasp/sling muscle fiber complex (the upper gastric sphincter) is related to the development of GERD (12, 15).

The aim of the current study is to expand the knowledge available on the individual anatomic components of the proximal stomach and distal esophagus and how these components combine to form the HPZ anti-reflux barrier. The defined structures evaluated were the clasp muscle fibers, sling muscle fibers, muscles within the esophagus in the area between the clasp/sling muscle fiber complex and LEC fibers, and the muscle fibers within the mid-esophagus. EUS was used *in vivo* and the relative distances and the muscular thickness of each structure were measured. Pressures were recorded and compared in each of these individual anatomic structures. Lastly, these same structures were identified, and their anatomical relationships measured, in specimens collected from organ donors using *ex vivo* high-resolution micro-computed tomography (micro-CT) scans.

Materials and Methods

IRB approval

Approval for this study was granted by the Institutional Review Board at Temple University Hospital (TUH), and all procedures and study protocol were in accordance with the policies of TUH and the National Institutes of Health (NIH).

Simultaneous Endoscopic Ultrasound (EUS) and Manometry

A total of 20 subjects undergoing endoscopy and EUS for non-esophageal disorders were evaluated, ranging in age from 30–76 (mean age ± standard error of mean 52 ± 2.4). There were seven males (age 59 ± 4.2) and thirteen females (age 49 ± 2.6). Subjects were excluded from the study if they had a history of esophagitis, heartburn, GERD, regurgitation, hiatal hernia, dysphagia, odynophagia, surgery involving the stomach or esophagus, scleroderma, esophageal dysmotility, achalasia, or current pregnancy. In accordance with policies of TUH and the NIH, all subjects provided informed consent to take part in this study. The indications for EUS were abdominal pain (2), abnormal imaging (4), pancreatitis (3), gastric mass not near the gastroesophageal junction (6), duodenal mass (1), pancreatic mass (3), pancreatic cyst (1).

The study was performed in a tertiary care setting. Subjects were sedated with midazolam and fentanyl titrated to the subject's anesthesia requirements. The subjects underwent EUS of the esophagus and stomach with an Olympus GF-UE160-AL5 Radial Endoscope (Olympus America Inc., Melville, NY, USA). The endoscope has an ultrasound transducer with a frequency of 7.5–10 MHz. The ultrasound images were recorded at a rate of 30 frames s^{-1} and the manometry was recorded at 250 Hz with the Kay Elemetrics Digital Swallowing Workstation Version 3.0.1 (Kay-Elemetrics, Lincoln Park, NJ, USA). A pull-through motor was used to pull the EUS endoscope through the proximal stomach and distal esophagus at a rate of 5 mm s^{-1}. Pressures were measured with a manometry catheter inserted through the biopsy channel of the EUS endoscope and placed at the level of the ultrasound transducer. A balloon at the end of the EUS endoscope was used to gain acoustic coupling and to compress the manometry catheter against the wall of the esophagus. The axial length of the balloon is 1.5 cm and it was inflated with water ranging from 1 ml to 2 ml. The balloon increased the measured pressure due to compression against the anatomic structures that generate the pressure. The volume of the balloon was kept constant during each pull-through. Several EUS and pressure readings were recorded simultaneously for each subject; however, data from inadequate pull-throughs or poor ultrasound imaging were not incorporated into the data set.

Distances between structures were calculated using the rate at which the pull-through was performed. These calculations were performed to determine where the structures were positioned in relation to when the right crural diaphragm (RCD) first comes in contact with the esophagus (Figure 1A). Distances were calculated for the beginning of the structure on ultrasound imaging, average maximal thickness, and end of the structure on ultrasound imaging. The values collected for each structure were averaged over the 20 patients.

The thickness of structures was obtained by taking measurements on two-dimensional cross-sectional ultrasound images of the inner circular smooth muscle layer for each structure. Each image was calibrated using the range and the ratio of pixels (horizontal to vertical) on the ultrasound image, using ImageJ software (National Institutes of Health, Bethesda, Maryland, USA). Thickness of the circular smooth muscle layers at different areas was calculated along a radial line from the center of the lumen. The measurements were obtained at the thickest segment on each individual cross sectional image.

In addition to evaluating the ultrasound images of the individual structures, the pressures generated by the individual structures were evaluated and compared to each other. The relative pressure values between structures were used in this study rather than the absolute pressure values, because pressures were increased to a variable extent due to the compression of the balloon against the pressure catheter and the esophageal wall. The distances of peak pressures were measured from the beginning of the upslope of the pressure curve in the cardia during a pull through from the stomach into the esophagus.

Statistical analyses of the above data were performed using Student's t-test. A p-value of <0.05 was considered significant. Measurements were reported as the mean ± standard error of the mean.

High-Resolution Micro-CT Scan of the gastroesophageal junction (GEJ)

Two specimens of human stomach and esophagus were obtained from organ procurement agencies (National Disease research Institute and the International Institutes for the Advancement of Medicine). The first specimen was prepared by filling with molten paraffin, then cooling on ice and fixing the specimen by submersion in 4% paraformaldehyde for 10 days. After fixative wash out using running tap water for several hours, the specimen was immersed in a 2% phosphotungstic acid, 0.02% potassium permanganate, 0.1% hematoxylin (PTAH) solution for 48 hours. The specimen was removed carefully from the paraffin mold, washed and then dissected down in size so that a region of 5 cm diameter × 5 cm in height remained that contained the clasp, sling and LEC together. This block of tissue was placed onto a piece of Styrofoam that was shaped to match the shape of the paraffin wax mold. The second specimen was prepared by cannulating the esophagus with a multi perforated 5 mm diameter tube, filling the stomach with a natural sponge soaked in the HTK transport media and shaped to match the shape of the gastric cardia then perfusing the specimen from the cannulation tube with 6 liters of 4% paraformaldehyde over 15 minutes, immersing the entire specimen. The specimen was then allowed to immersion fix for 10 days, washed extensively with tap water, immersed in PTAH for 48 hours, washed and processed as described above. The tissue blocks with the Styrofoam "mount" were wrapped several times in Parafilm, with pieces of damp Kimwipe included at the bottom of this wrapped tissue block, in order to maintain constant moisture within the sample during the subsequent scans.

For the micro-CT, a SkyScan 1172 high-resolution cone-beam micro-CT scanner (SkyScan, Ltd, Kontich, Belgium), with a Hamamatsu C9300 11Mp camera, was used to scan the specimens using the double-side and oversize sample options. The following settings were used: a camera pixel size of 8.76 μm, an image pixel size of 11.89 μm, voltage of 80 kV, current of 124 μA, aluminum 0.5mm as well as copper filters, rotation step of 0.50 degrees, 180 degrees of rotation, a frame averaging of 8, 1,335 rows, 3,872 columns, and a scan duration of 3 hours and 45 minutes. The image slices were reconstructed using cone-beam reconstruction software (SkyScan NRecon) based on the Feldkamp algorithm, on 3 linked servers, a process that yielded 3492 tomographic sections, each with a thickness of 11.89 μm in the axial (transverse) plane, for each sample. A ring artifact correction of 10, and a beam hardening correction of 40% was applied to both samples. Three dimensional (3D) image constructs were made using 3D imaging software (SkyScan CTVox, Figure 4). Virtual dissection of these 3D constructs was performed in order to image the clasp and sling fibers of the stomach (see Figure 4A), using sphere-shaped and cylinder-shaped virtual "cutting boxes".

Next, using the Skyscan CT Analyzer software (CTAn), the portion of the esophagus that stretched from the cardiac notch cephalad for 35 mm was virtually divided into 22 different regions. Each selected region was 10 slices in height (118.9 μm or 0.01 mm), and separated from the next region by 1.5 mm. Examples of these virtual dissections are shown in Figure

4B. In each of the 22 regions, the circular smooth muscle layer of the esophagus was segmented out (delineated) from the other layers using a region of interest tool that is part of the CTAn software (see Figure 4C), binarized and saved separately as 22 different volumes of interest. The mean cross-sectional thickness of the circular smooth muscle was then calculated (in mm) for each of the 22 volumes of interest, and plotted with distance from the cardiac notch as the X-axis.

Results

Anatomy of the clasp, sling and LEC fibers using simultaneous EUS and manometry

When imaged in cross-section, an asymmetric thickening in the area of the cardia is evident on the greater curvature of the stomach. These muscle fibers are defined as sling fibers (Figure 1A). The clasp muscle fibers appear as a thinner group of muscle fibers on the lesser curvature side of the stomach, which bridge and connect the two arms of the sling fibers. In addition, the crural diaphragm can be clearly demonstrated on EUS as two distinct muscle bands compressing the esophageal wall (Figure 1A).

In 10 of the 20 subjects, the RCD was the first portion of the crural diaphragm to compress the esophagus. In 2 subjects, the left crural diaphragm (LCD) was the first portion of the crural diaphragm to compress the esophagus. In 8 subjects, the right and left crus appeared to compress the esophagus at the same location. The beginning of the clasp and sling muscle fibers first appears at a distance of 13.8 ± 2.4 mm distal to the distal most point at which the RCD contacts the esophagus. The average maximal thickness of the clasp and sling muscle fibers appears at a distance of 3.4 ± 2.8 mm distal from the distal contact between the RCD and the esophagus. The proximal end of the clasp and sling muscle fibers appears at a distance of 16.8 ± 2.4 mm proximal to the distal most point of contact of the RCD with the esophagus. The average axial length of the clasp and sling muscle fibers in the longitudinal axis is 30.3 ± 3.0 mm (Figure 2A). The beginning of the LEC appears at 41.3 ± 3.4 mm, the maximal thickness appears at 56.2 ± 5.2 mm, and the end of the LEC appears at of 75.7 ± 5.9 mm all measured from the distal most point of contact of the RCD with the esophagus. The average length in the longitudinal axis of the LEC is 34.4 ± 3.7 mm (Figure 2A).

Results of the average maximum thickness of the different muscle fibers are shown in figure 2B. The sling and LEC fibers are statistically significantly thicker than the other three muscle groups ($p<0.01$). The clasp fibers are statistically significantly thicker than the esophageal wall in the area between the clasp and sling muscle fiber complex ($p<0.05$).

Comparison of peak pressures using simultaneous EUS and manometry

There are three pressure peaks (Figure 3). The distal pressure peak is generated by the clasp/sling muscle complex, the middle peak is due to the crural diaphragm and the proximal peak is due to the LEC muscle fibers. The pressure generated by the LEC has a distinct bimodal contour in 9/20 subjects (Figure 3A). The average peak pressures were 19.1 ± 4.2 mmHg for the clasp/sling fiber complex, 23.3 ± 5.6 for the crural diaphragm and 53.0 ± 7.1 for the LEC. The peak pressure at the LEC muscle fibers is statistically significantly greater than at the either the crural diaphragm or the clasp/sling fiber complex ($p<0.001$, ANOVA with Student-Newman-Keuls posthoc tests).

The ultrasound images were imported into the SkyScan NRecon software so that three dimensional reconstructions of the ultrasound images in the area of the LEC could be used to demonstrate that there are two areas of thickened muscle within the LEC in 9 subjects (Figure 1B-E). The remaining 11 subjects showed a single pressure peak at LEC. Patients showing 2 pressure peaks at the LEC are statistically significantly older than patients with only 1 pressure peak (59 ± 3.3 vs 47 ± 2.3 years). There is no relationship between the

clinical indication for ultrasonography and whether 1 or 2 pressure peaks at the LEC were observed. Representative pressure traces for both these patterns are shown in figure 3. The SkyScan NRecon software cutting box tools were used to virtually dissect the three dimensional reconstructions. A video of this virtual dissection in AVI format is available as supplementary video 1 on the journal web site.

Anatomical relationships revealed by Micro-CT

Virtual dissection of the micro-CT images reveals that the anatomical relationships of the GEJ muscle groups are consistent with the anatomy of the clasp and sling muscle fiber complex determined by EUS and manometry. The sling fibers are visualized as a band of thickened muscle on the greater curvature side of the stomach surrounding the distal esophagus in a sling like fashion (Figure 4A). When imaged in cross-section, the sling fibers are thicker on the greater curvature side of the stomach and thin towards the lesser curvature side of the stomach. The clasp fibers appear as a thinner group of muscles that bridge and connect the two arms of the sling fibers. As seen on cross-sectional images, this appears as a thinner portion of muscle within the cardia on the lesser curvature side of the stomach.

Virtual dissection of the micro-CT images also reveals that there are two areas of thickened muscle within the LEC (Figure 4B, C and Figure 5), results that are consistent with the results of the EUS and manometry. Axial micro-CT images of the esophagus shown in Figure 4B shows thickened circular smooth muscles (arrows) at 33.8 mm cephalad of the cardiac notch. This thickening is still present at 33.1 mm. The circular smooth muscle layer is quite thin thereafter, down to approximately 100 mm cephalad to the cardiac notch (see Figure 4B images from 25 mm to 13.4 mm). By 8.4 mm cephalad to the cardiac notch, the circular muscle thickens again (indicated by arrows in this slice). The circular smooth muscle was then segmented from the other layers using a region of interest tool in the analysis software (see methods), as shown in Figure 4C. The mean cross-sectional thickness of the circular smooth muscle was then calculated, and is shown in Figure 5. Two areas with thickened circular smooth muscles are detected, at 7.5 mm and at 30–33.5 mm cephalad to the cardiac notch.

Discussion

In the current study, we show the various anatomic structures, their configurations, sizes and relative locations within the GEJHPZ. We also show the pressure changes that these anatomic structures generate by using EUS, combined with manometry.

The present study differs from our prior reports in a number of important ways. First, regarding the methodology, the ultrasound transducer that was used in the current study was a 7 to 10 mHz ultrasound scope. The transducers used in our previous studies were 20 mHz ultrasound probes. The lower frequency increased the penetration of the ultrasound waves. An increase in the size of the aperture greatly increased the resolution of the ultrasound image. This increase in penetration and resolution made it easier to see the beginning and the end of the crural diaphragm on both the left and the right side. This also made it possible to image the clasp and sling muscle fibers that were not previously imaged using the probe system. In the previous studies, the clasp and sling muscle fibers were implied by the pressure profile that they generated. Second, the use of the balloon around the ultrasound transducer made it possible to image the clasp and sling fibers directly by providing reliable acoustic coupling of the ultrasound scope to the wall of the esophagus. In addition, the balloon acted as a bolus, allowing clear demarcation of the pressure profile from the various structures. The balloon prevented air from interfering with acoustic coupling by providing a fluid filled medium for conduction of the ultrasound waves. These refinements allowed us

for the first time to make precise measurements of the thickness of the clasp and sling muscle fibers, the crural diaphragm and the LEC in vivo.

We found that the most distal muscle group of the HPZ, located within the cardia of the stomach, represents the gastric clasp and sling muscle fiber complex. The second more proximal HPZ component represents the pressure profile generated by the crural diaphragm. This component was visualized using EUS but not on the micro-CT scan, because the crural diaphragm was dissected off during removal of the stomach and the esophagus from the body. The most proximal HPZ component represents the LEC on EUS. This muscle group appears as a thickened circumferential band of muscle on EUS, above the crural diaphragm and generates a high pressure on manometry. The LEC is clearly demonstrated at a separate location from both the clasp/sling muscle fiber complex and the crural diaphragm. In 9 of the 20 subjects, this muscle group generated a bimodal pressure peak which correlated with two areas of thickened muscle within the LEC. It is likely that the distention generated by the balloon allowed us to demonstrate the bimodal pressure peaks within the LEC, which has not previously been described. In the other 11 subjects there was a single peak that correlated with a single area of thickened muscle within the LEC.

The micro CT data presented is completely new and unique. This technology allows virtual dissection in any plane and at any angle desired producing a superior description of the area of the GEJHPZ than was ever before possible using physical dissection of the area. During actual dissection, once the tissue is cut, it is destroyed, and there is no way to go back and cut it again. With virtual dissection we are able to cut the tissue, evaluate it, and then re-cut the tissue as many times as necessary, without destroying the tissue. The sling muscle fiber group appears as a thickened band of muscle within the cardia of the stomach draping over the greater curvature of the stomach much like a sling. The clasp muscle fibers appear as a thinner more diffuse muscle group on the lesser curvature side of the stomach connecting both sides of the sling muscle, pulling (clasping) the two sides of the sling muscle together. The micro-CT scan images are consistent with high-resolution ultrasound images in the 20 subjects included in the EUS imaging study. Simultaneous ultrasound and manometry was used to demonstrate pressure profiles generated by the components of the GEJHPZ.

The normal physiology of the GEJ is not only important to understand in and of itself, but also because of the implications that it has on understanding GERD (2, 15). At the GEJ, a number of structures contribute to the HPZ. There are several theories regarding these structures and their contributions to the HPZ. One theory is that the clasp and sling muscle fiber complex, in conjunction with the crural diaphragm, prevent the reflux of gastric contents into the esophagus (14, 16, 17). Another theory is that the intrinsic circular smooth muscle of the LEC and the crural diaphragm skeletal muscle prevent reflux (4, 6, 8, 9). These two theories were considered mutually exclusive until we showed three distinct areas of high pressure within the HPZ, and proposed that these three pressure peaks correspond to the gastric clasp and sling muscle fiber complex, the crural diaphragm, and the LEC (12). These findings and the findings in the current study indicate that the HPZ of the distal esophagus actually consists of a combination of the components represented in the two previous theories.

The sling muscle fiber group appears as a thickened band of muscle within the cardia of the stomach draping over the greater curvature of the stomach much like a sling. The clasp muscle fibers appear as a thinner more diffuse muscle group on the lesser curvature side of the stomach connecting both sides of the sling muscle, apparently pulling (clasping) the two sides of the sling muscle together. The micro-CT scan images are consistent with high-resolution ultrasound images in the 20 subjects included in the EUS imaging study. Simultaneous ultrasound and manometry was used to demonstrate pressure profiles

generated by the components of the GEJHPZ. The second more proximal HPZ component represents the pressure profile generated by the crural diaphragm. This component was visualized using EUS but not on the micro-CT scan, because the crural diaphragm was dissected off during removal of the stomach and the esophagus from the body.

McCray *et al.*, demonstrated that the LEC and crural diaphragm are 8.3 ± 5.9 mm apart during maximal end inspiration. These findings, that the LEC and crural diaphragm are two distinct structural entities, are also consistent with our current data (18). The average maximal thicknesses of the structures were measured to better understand the anatomy and their relationship to each other. The sling muscle fiber thickness is statistically significantly greater than the thickness of the muscle within the esophageal wall between the clasp and sling muscle fiber complex and the LEC. The sling muscle fiber thickness is also statistically significantly greater than the muscle within the wall of the mid-esophagus. Furthermore, the average maximal sling muscle fiber thickness is statistically significantly less than the LEC. We also demonstrated that the thickness of the LEC is greater than the adjacent muscle within the wall of the mid-esophagus. Again, this highlights the LEC as a distinct anatomical and physiological site within the HPZ. The pressure profiles also support our earlier findings of distinct and separate areas of high pressure within the HPZ, areas that also correspond to distinct and separate anatomic structures as determined by EUS imaging (12).

The thickness of the circular muscle within the esophageal wall in the area between the clasp and sling muscle fiber complex and the LEC is statistically significantly less than the thickness of the LEC, even in the area above the crural diaphragm where the diaphragm does not compress the wall of the esophagus. This is a new finding. The pressure between the crural diaphragm and the LEC was relatively low, suggesting that the intrinsic smooth muscle in the wall of the esophagus at this area does not act as a sphincter and does not contribute directly to the anti-reflux barrier of the HPZ. Compression from the crural diaphragm increases the luminal pressure generated in this area and appears to be the only pressure-generating structure at this location.

As already mentioned, the balloon around the ultrasound transducer artificially increases the pressure from the pressure generating structures within the HPZ. The esophageal wall was somewhat distended by the balloon and we were able to detect the pressure generated by the individual structures within the HPZ that may not have been obvious without the use of the balloon or may have required the use of pharmacologic agents to separate the pressure profiles, as in our prior studies. However, the thickness of the intrinsic structures within the wall of the esophagus may have been slightly distorted. Nevertheless, the balloon was kept at the same volume for each individual subject. Therefore, the relative thicknesses of these structures are still accurately represented. The water-distended balloon was necessary for acoustic coupling in many of the subjects. Without balloon distension, image quality suffered such that the ultrasound measurements could not be taken.

In conclusion, there are three separate and distinct anatomic regions that contribute to the HPZ within the distal esophagus: the clasp and sling muscle fiber complex at the gastric cardia, the crural diaphragm, and the LEC. There is a distinct increase in the thickness and pressure at the LEC that does not overlap the crural diaphragm. The LEC consists of thickened muscle, which often generates a bimodal pressure peak. Additionally, the LEC generates the greatest pressure of all of the individual HPZ components (12). In the future, we plan to apply the methods used in this study to evaluate subjects with GERD and hiatal hernia.

Supplementary Material

Refer to Web version on PubMed Central for supplementary material.

Acknowledgments

Grant Support: This project was supported by Award Number R01 DK079954 from the National Institute of Diabetes and Digestive and Kidney Diseases. The content is solely the responsibility of the authors and does not necessarily represent the official views of the National Institute of Diabetes and Digestive and Kidney Diseases or the National Institutes of Health.

References

1. Dent J, El-Serag HB, Wallander MA, Johansson S. Epidemiology of gastro-oesophageal reflux disease: a systematic review. Gut. 2005; 54:710–717. [PubMed: 15831922]
2. Code CF, Fyke FE Jr, Schlegel JF. The gastroesophageal sphincter in healthy human beings. Gastroenterologia. 1956; 86:135–150. [PubMed: 13384582]
3. Ingelfinger FJ. Esophageal motility. Physiol Rev. 1958; 38:533–584. [PubMed: 13590930]
4. Dodds WJ, Dent J, Hogan WJ, Arndorfer RC. Effect of atropine on esophageal motor function in humans. Am J Physiol. 1981; 240:G290–G296. [PubMed: 6784581]
5. Fang JC, Sarosiek I, Yamamoto Y, Liu J, Mittal RK. Cholinergic blockade inhibits gastro-oesophageal reflux and transient lower oesophageal sphincter relaxation through a central mechanism. Gut. 1999; 44:603–607. [PubMed: 10205193]
6. Holloway RH, Dodds WJ, Helm JF, Hogan WJ, Dent J, Arndorfer RC. Integrity of cholinergic innervation to the lower esophageal sphincter in achalasia. Gastroenterology. 1986; 90:924–929. [PubMed: 3949120]
7. Mittal RK, Chiareli C, Liu J, Holloway RH, Dixon W Jr. Atropine inhibits gastric distension and pharyngeal receptor mediated lower oesophageal sphincter relaxation. Gut. 1997; 41:285–290. [PubMed: 9378379]
8. Mittal RK, Fisher M, McCallum RW, Rochester DF, Dent J, Sluss J. Human lower esophageal sphincter pressure response to increased intra-abdominal pressure. Am J Physiol. 1990; 258:G624–G630. [PubMed: 2333975]
9. Mittal RK, Holloway R, Dent J. Effect of atropine on the frequency of reflux and transient lower esophageal sphincter relaxation in normal subjects. Gastroenterology. 1995; 109:1547–1554. [PubMed: 7557138]
10. Kahrilas PJ. Anatomy and physiology of the gastroesophageal junction. Gastroenterol Clin North Am. 1997; 26:467–486. [PubMed: 9309398]
11. Liu JB, Miller LS, Goldberg BB, et al. Transnasal US of the esophagus: preliminary morphologic and function studies. Radiology. 1992; 184:721–727. [PubMed: 1509056]
12. Brasseur JG, Ulerich R, Dai Q, et al. Pharmacological dissection of the human gastro-oesophageal segment into three sphincteric components. J Physiol (Lond). 2007; 580:961–975. [PubMed: 17289789]
13. Liebermann-Meffert D, Allgower M, Schmid P, Blum AL. Muscular equivalent of the lower esophageal sphincter. Gastroenterology. 1979; 76:31–38. [PubMed: 81791]
14. Gonzalez AA, Farre R, Clave P, Gonzalez AA, Farre R, Clave P. Different responsiveness of excitatory and inhibitory enteric motor neurons in the human esophagus to electrical field stimulation and to nicotine. Am J Physiol Gastrointest Liver Physiol. 2004; 287:G299–G306. [PubMed: 15016616]
15. Miller L, Dai Q, Vegesna A, et al. A missing sphincteric component of the gastro-oesophageal junction in patients with GORD. Neurogastroenterol Motil. 2009; 21:813–e852. [PubMed: 19368661]
16. Stein HJ, Liebermann-Meffert D, DeMeester TR, Siewert JR. Three-dimensional pressure image and muscular structure of the human lower esophageal sphincter. Surgery. 1995; 117:692–698. [PubMed: 7778032]

17. Tian ZQ, Liu JF, Wang GY, et al. Responses of human clasp and sling fibers to neuromimetics. J Gastroenterol Hepatol. 2004; 19:440–447. [PubMed: 15012783]
18. McCray WH Jr, Chung C, Parkman HP, Miller LS. Use of simultaneous high-resolution endoluminal sonography (HRES) and manometry to characterize high pressure zone of distal esophagus. Dig Dis Sci. 2000; 45:1660–1666. [PubMed: 11007121]

Abbreviations used

EUS	Endoscopic ultrasound
GEJ	Gastroesophageal Junction
GEJHPZ	Gastroesophageal Junction High-Pressure Zone
GERD	Gastroesophageal Reflux Disease
HPZ	High-Pressure Zone
LCD	Left Crural Diaphragm
LEC	Lower esophageal circular sphincter
micro-CT	Micro-computed tomography
NIH	National Institutes of Health
PTAH	PhosphoTungstic Acid, Hematoxylin
RCD	Right Crural Diaphragm
TUH	Temple University Hospital

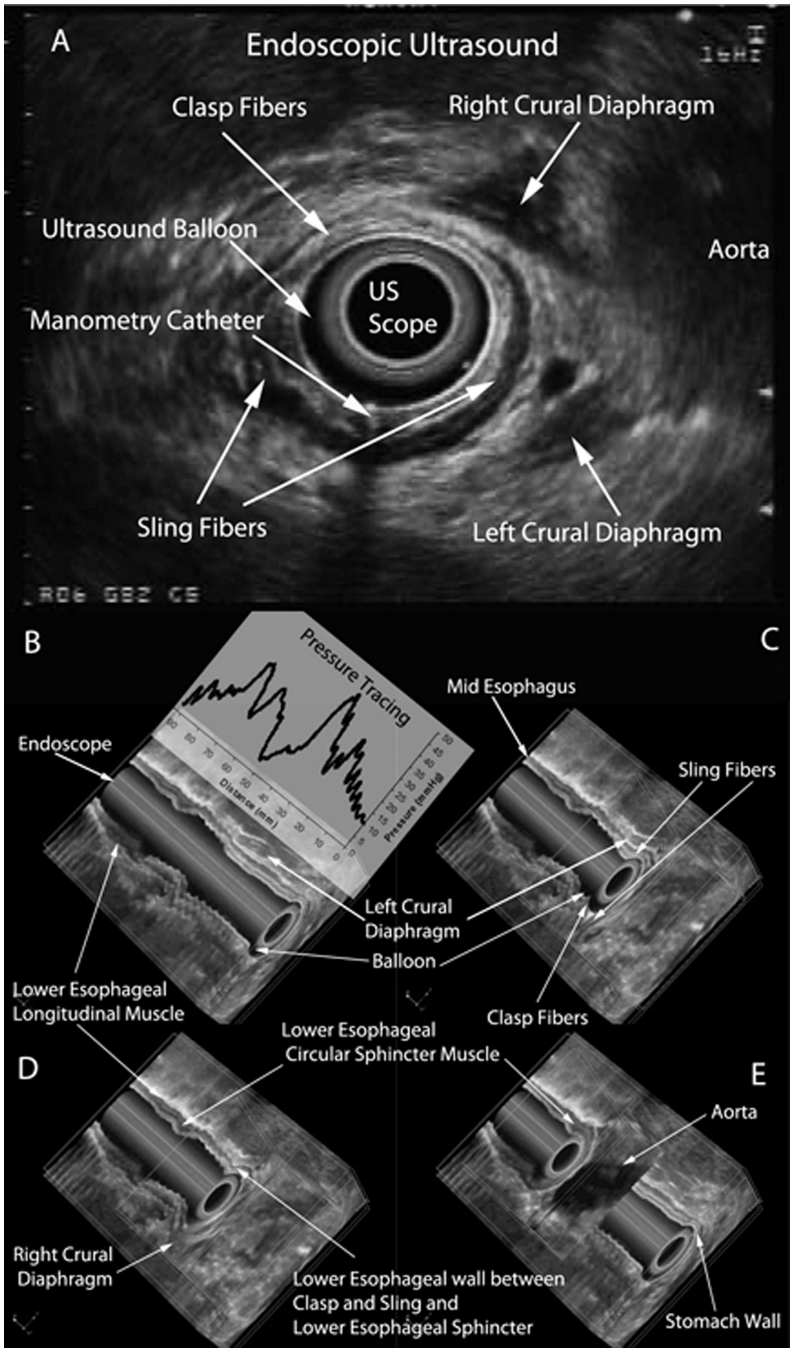

Figure 1.

(A) Endoscopic ultrasound image showing left and right crural diaphragm, clasp fibers, sling fibers, aorta, ultrasound scope, ultrasound balloon and the manometry catheter outside the ultrasound balloon. Panels B-E illustrates four different images of a 3-dimensional (3D) reconstruction of the 2-dimensional (2D) endoscopic ultrasound pull-through shown in panel A. The images are oriented such that the anterior surface of the patient is facing upward and the structures viewed on the anterior surface are in a coronal plane. The images are also oriented such that the stomach is inferior and the proximal esophagus is superior. (B-E) The 3D reconstruction is rotated to show the axial plane at the same time as the anterior surface. The wavy nature of the mucosal surface and artifacts passing through the entire coronal

plane may be due to pulsations from the heart and aorta which were transmitted to the esophagus and the endoscope during image acquisition. (B) The entire 3D reconstruction is shown before a cutting box was used as a virtual dissection tool. The column that extends through the image is the endoscope. Virtual dissection was performed to the level of the endoscope, so internal structures could be seen. The hypo-echoic area, signified by black, surrounding the endoscope is the balloon on the endoscope. The pressure profile obtained from the manometry catheter is also shown in this image. (C) The cutting box is shown as it virtually dissects the 3D reconstructed image to the clasp and sling fibers. The cutting box allows for structures to be visualized in the coronal and axial planes. (D) The progression of the cutting box is shown as it moves from the stomach towards the mid-esophagus. During this progression the right crural diaphragm (RCD) is visualized. (E) The lower esophageal circular muscle fibers, both in the coronal and axial planes can be visualized. The cutting box also shows the aorta posterior to the esophagus.

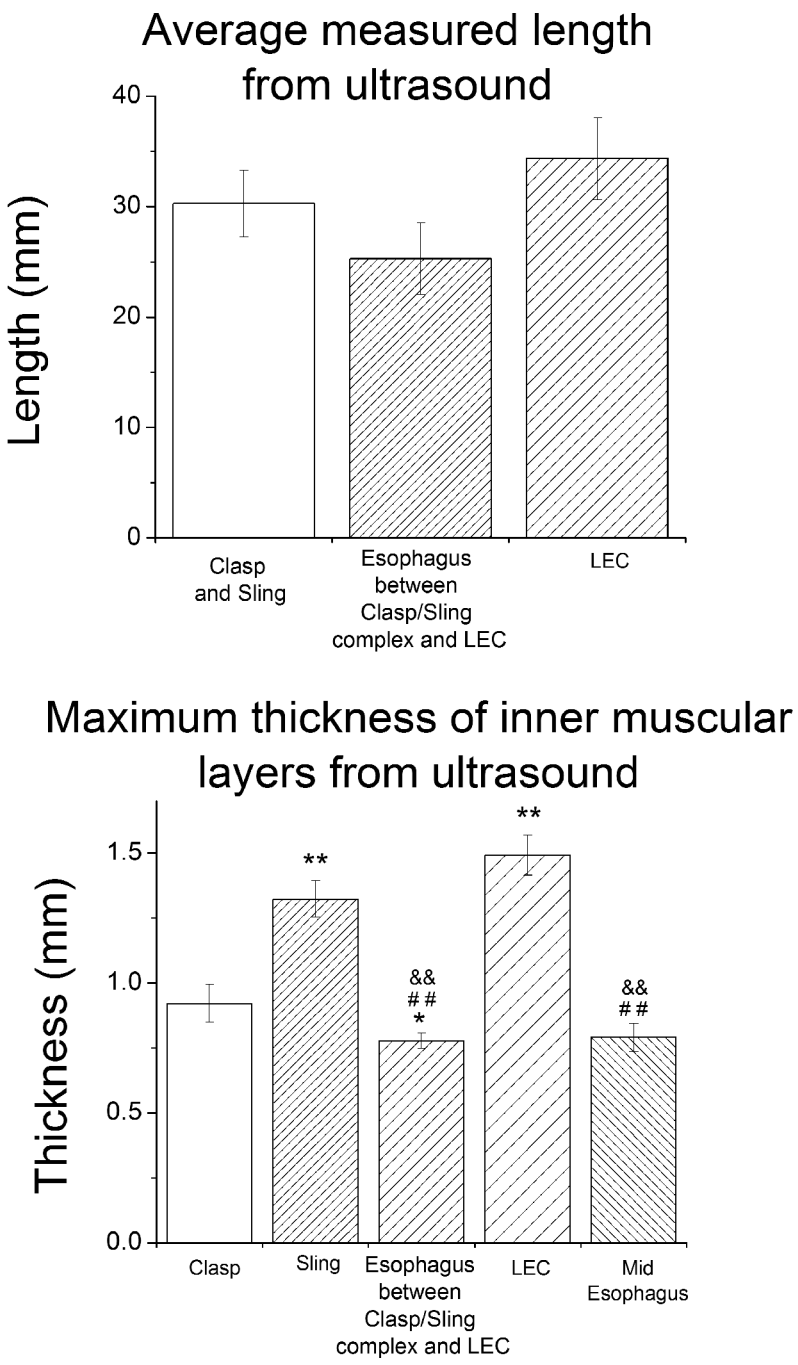

Figure 2.

(A) Average measured length of structures in the axial direction. (B) Maximum cross-sectional thickness (mm) of structures determined using endoscopic ultrasound. Data is shown as mean ± sem. ** Statistically significantly different from clasp ($p<0.01$); * statistically significantly different from clasp ($p<0.05$); # # statistically significantly different from sling ($p<0.01$); & & statistically significantly different from LEC ($p<0.01$).

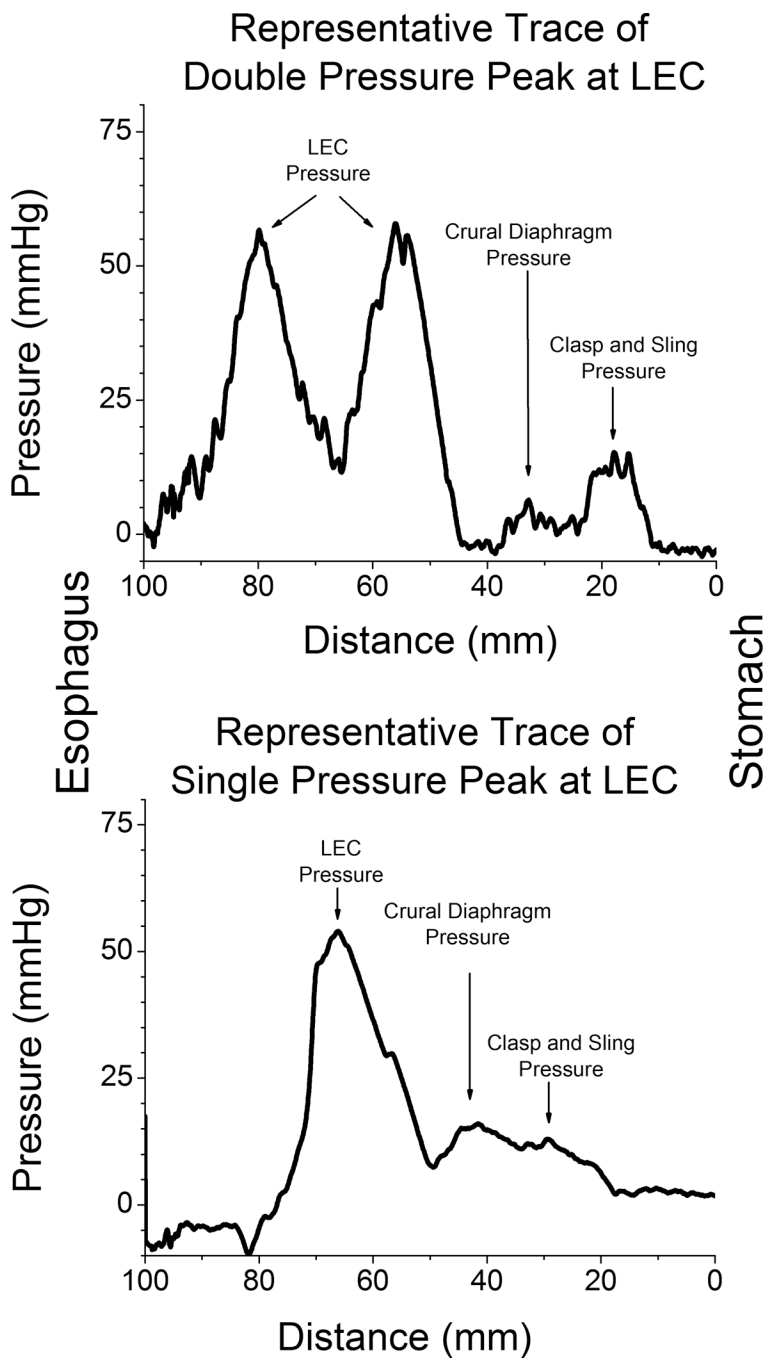

Figure 3.
(A) Representative trace of the pressure generated during a pull through in a subject showing double pressure peaks at the lower esophageal circular muscle fibers. (B) Representative trace of the pressure generated during a pull through in another subject showing single pressure peaks at the lower esophageal circular muscle fibers.

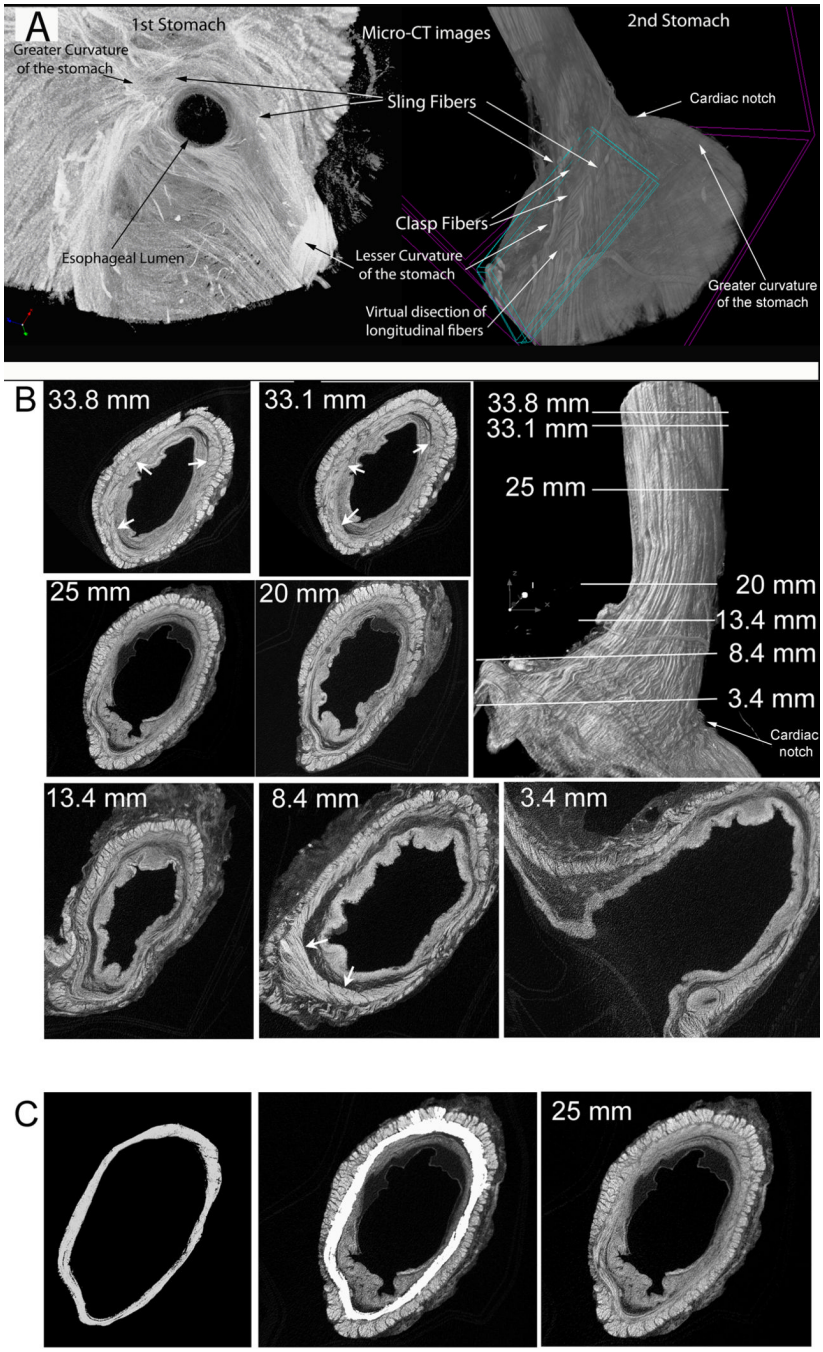

Figure 4.

(A) Micro-CT images showing clasp and sling muscle fibers from two different stomach and esophagus specimens procured from organ donors. The image on the left is a view from the inside of the stomach after virtually dissecting the mucosa. The sling fibers can be observed encircling more than 75% of the esophageal lumen and then running along the lesser curvature. The image on the right is a view from the outside of the stomach and esophagus after virtually dissecting the longitudinal muscle fibers along the lesser curvature. The sling fibers can be seen running longitudinally and being bridged by the clasp fibers. (B) Micro-CT images from the second organ donor stomach illustrating the changes in thickness of inner circular smooth muscle layer of the esophagus. Upper right image is a view of the

entire specimen with the greater curvature of the stomach at the bottom right and the lesser curvature at the bottom left. Numbers refer to the cross section images and distances are measured in mm from the cardiac notch. (C) Illustration of the method used to determine the thickness of the inner circular smooth muscle layer at 25 mm from the cardiac notch. SkyScan software was used to trace the circular smooth muscle layer boundaries on the image at the right. The image on the left shows the virtually dissected smooth muscle layer. The middle image is merged from left and right images with the inner circular smooth muscle layer colored in white.

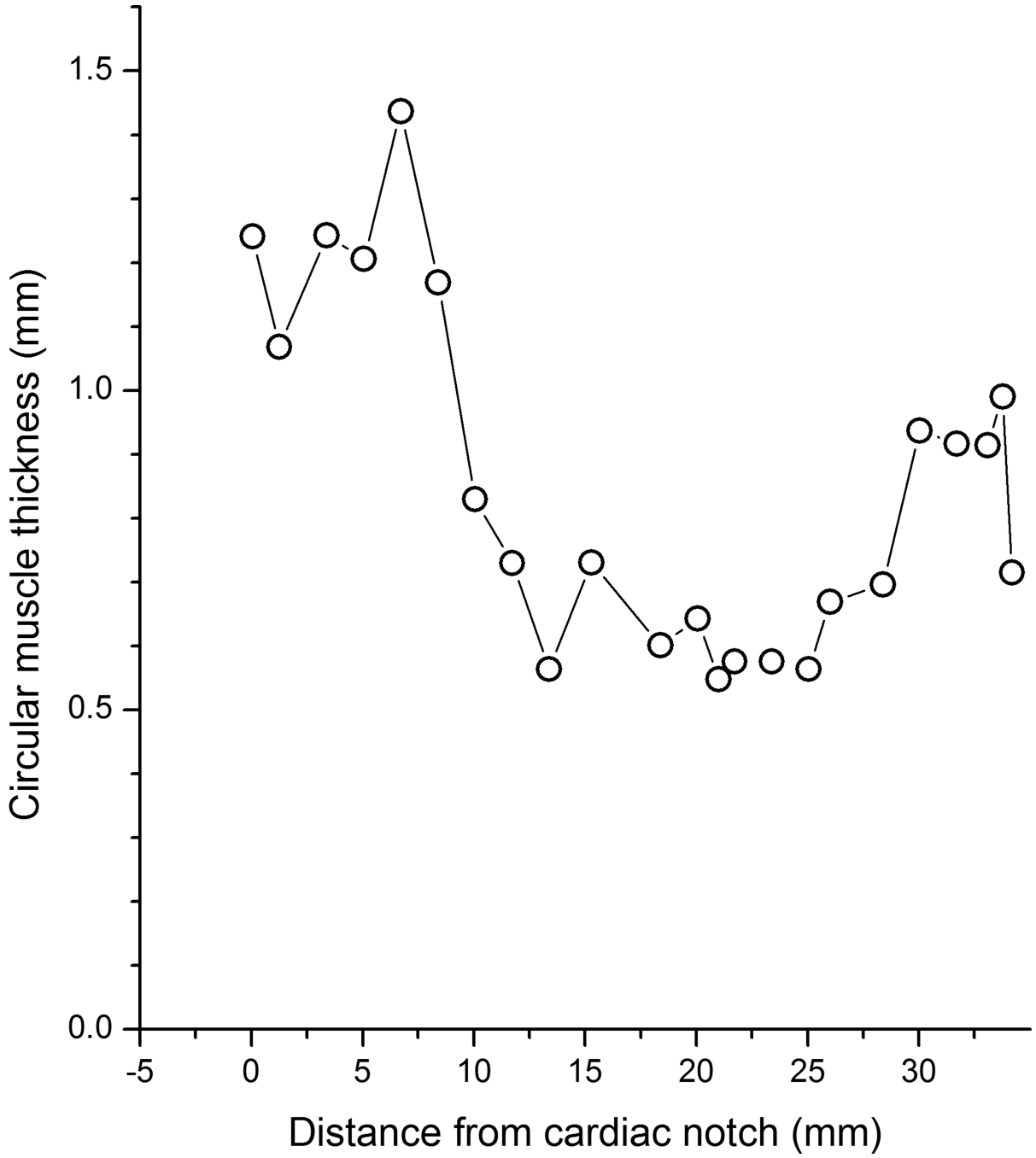

Figure 5.
Plot of the thickness of the circular smooth muscle layer determined by μCT as illustrated in figure 4B. The circular smooth muscle layer is thickest near the cardiac notch (clasp and sling fibers) and decreases to a minimum between 10 and 25 mm from the cardiac notch then increases coincident with the lower esophageal circular smooth muscle sphincter.